Journal of Aerosol Science 114 (2017) 250–262

Contents lists available at ScienceDirect

Journal of Aerosol Science

journal homepage: www.elsevier.com/locate/jaerosci

Screen collection efficiency of airborne fibers with monodisperse length

Bon Ki Ku*, Gregory Deye, Leonid A. Turkevich

Centers for Disease Control and Prevention (CDC), National Institute for Occupational Safety and Health (NIOSH), Division of Applied Research and Technology (DART), 1090 Tusculum Ave, MS-R7, Cincinnati, OH 45226, USA

ARTICLE INFO

Keywords:
Glass fiber
Fiber length
Nylon mesh screens
Collection efficiency

ABSTRACT

Fiber length is believed to be an important variable in determining various toxicological responses to asbestos and other elongate mineral particles. In this study we investigated screen collection characteristics using monodisperse-length glass fibers (i.e., 11, 15, 25, and 53 μm in length), to better understand the collection of fibers with different lengths on screens with different mesh sizes. A well-dispersed aerosol of glass fibers (geometric mean length ~ 20 μm), generated by vortex shaking, was fed directly into the Baron Fiber Length Classifier, in order to produce monodisperse length fibers. With nylon mesh screens (10, 20, 30, 41 and 60 μm mesh sizes), the screen collection efficiency was measured using an aerodynamic particle sizer. As the screen mesh size decreases from 60 μm to 10 μm, the screen collection efficiency for 53 μm fibers increases (from 0.3 to 0.9) while 11 μm fibers exhibited a collection efficiency independent of screen mesh size. The collection efficiency for the longest fibers was found to be nearly constant for aerodynamic diameters 1–4 μm for screens 20 and 30 μm, but to rise significantly at aerodynamic diameters larger than 4 μm. For the 20 μm screen, the collection efficiency for fibers with lengths > 20 μm is a factor of two to five larger than that for spherical particles with the same aerodynamic diameter. We believe that fibers are collected on the screen primarily by interception below 4 μm in aerodynamic diameter, and by impaction above 4 μm. This study represents a fundamental advance in the understanding of the interaction of screens with a fibrous aerosol.

1. Introduction

Understanding fiber deposition in the respiratory system is of great interest to elucidate the adverse health effects of inhaled fibrous particles (Baron, 2001; Hesterberg & Hart, 2001; Spurny, Stober, Opiela, & Weiss, 1979). In addition, NIOSH has advocated comprehensive research on airborne fibers, such as asbestos and elongated mineral particles (EMPs), in order to isolate the particular parameters of toxicity of these materials (NIOSH, 2011). Because fiber length has long been suspected as being a crucial parameter in determining various toxicological endpoints of asbestos and similar materials (Stanton et al., 1981), efforts have been made to study the deposition of airborne fibers in the respiratory system and in the filtration media as a function of fiber dimension (especially length). Related studies have been conducted on the deposition of fibrous particles in the human nasal/oral airways (Su & Cheng, 2005, 2006, 2009; Su, Wu, & Cheng, 2008) and on filtration media (Gentry & Spurny, 1978; Gentry, Spurny, Opiela, & Weiss, 1980; Gentry, Spurny, & Schoermann, 1989) in the submicrometer and micrometer size range for both asbestos and man-made fibers. Understanding the subtleties associated with the deposition of these materials on filter media is equally important for a proper

* Corresponding author.
E-mail address: bku@cdc.gov (B.K. Ku).

http://dx.doi.org/10.1016/j.jaerosci.2017.09.006
Received 17 January 2017; Received in revised form 3 May 2017; Accepted 5 September 2017
Available online 23 September 2017
0021-8502/ Published by Elsevier Ltd.

interpretation of air sampling.

Gentry and colleagues studied the collection efficiency of asbestos fibers using optical light scattering (Gentry & Spurny, 1978) and electron microscopy (Gentry et al., 1989). They reported a number of difficulties in measuring the collection efficiency of fibers on filters compared to isometric particles: (1) fiber samples typically have a wide range of lengths and diameters; (2) well-dispersed fibers are not easy to aerosolize from the bulk fiber samples, and the generated aerosol typically contains many agglomerates; (3) the collection efficiency on a substrate depends on fiber orientation. Interpretation of the optical scattering by fibers is complicated by the fiber orientational degree of freedom, so it is not straightforward to deconvolute fiber length from the scattering signal. Using electron microscopy to get fiber length and diameter distributions is time-consuming.

Ku and colleagues demonstrated a vortex shaking method to produce well-dispersed fibers from glass fiber powders (Ku, Deye, & Turkevich, 2013). A recent study has shown that screens with different apertures can remove longer fibers in the micrometer size range (Ku, Deye, & Turkevich, 2014); these authors suggest that screens can serve as a means to separate fibers by length. Myojo (1999) proposed a method for determining the length distribution of fibrous aerosol using an array of wire mesh screens. Chen, Wang, Bahk, Fissan, and Pui (2014) studied penetration of carbon nanotube (CNT) particles of mobility diameter 20–500 nm and their alignment through fibrous and electret filter media. Bahk, Buha, and Wang (2013) developed a method to determine CNT lengths by combination of mobility measurement and filtration model calculation. However, there is still little information available about how fiber length may influence screen collection efficiency. Thus, it is desirable to measure collection efficiency of screens in removing airborne fibers as a function of length and to characterize the aerodynamic behavior of the fibers during this process.

In this study we investigated screen collection efficiency of airborne glass fibers (a surrogate of asbestos) with monodisperse length. There were several aims to this study: 1) to determine the relation between screen collection efficiency and fiber length for given different mesh screens; and 2) to better understand the collection characteristics of fibers. To achieve this, monodisperse length fibers were prepared (in real time) by a dielectrophoresis-based Baron fiber length classifier (Baron, Deye, & Fernback, 1994; Deye, Gao, Baron, & Fernback, 1999). The length-selected fibers were used to obtain collection efficiency of screens with different mesh sizes by measuring upstream and downstream concentrations of the fibers using an aerodynamic particle sizer. The collection efficiency for fibers was compared to that of spherical particles for one screen.

2. Experimental methods

Glass fiber powder, supplied by Japan Fibrous Material Research Association (Kohyama, Tanaka, Tomita, Kudo, & Shinohara, 1997), was aerosolized (with geometric mean length of 20 μm, and, correspondingly, a mean length of 30.1 μm) by a vortex shaking method (Ku et al., 2013) and was provided, at 1.5 lpm, through a neutralizer (Po-210, 2 μCi), to the fiber length classifier (FLC). Characterization of the vortex generator system is described in detail in our recent study (Ku et al., 2013). The principle and operation of the FLC are described in the previous studies (Baron et al., 1994; Deye et al., 1999). Briefly, this classifier A (Fig. 1) isolates fibers of a chosen length through the process of dielectrophoretic mobility. Due to the electric field magnitude gradient, a neutral fiber experiences a net force in the annular region of the FLC (between the inner electrode and the outer tube). A 50-Hz A.C. potential of 0–10 kV peak-to-peak (square wave) is applied between the inner and outer electrodes to make fiber separation. In this alternating field, charged fibers oscillate about the trajectory predicted for dielectrophoretic motion. If the fibers would not be highly charged (the fibers are neutralized before the FLC), the oscillation would be sufficiently small that additional deposition and hence significant broadening of the classified fiber distribution would not occur, as shown in the previous studies. In practice, the product of the fiber length and the FLC voltage is roughly constant. Operated in the differential mode, the shortest fibers transit the length of the instrument and exit via the dump slot; the longer fibers are deposited on the inner electrode (rod); only a narrow range of intermediate length fibers are collected at the output of the instrument. For conductive long fibers, the dielectrophoretic velocity is proportional to the square of the fiber length (Lipowicz & Yeh, 1989). Aerosol and sheath flows are provided at 50% relative humidity (RH) to ensure conductivity of the glass fibers; this conductivity enables polarization and alignment of the fibers in the electric field (Wang et al., 2005).

The FLC-selected samples are sampled by the arrangement at C (Fig. 1). The filters may be changed by this arrangement without disturbing the classifier flow. The fiber samples were collected on a mixed cellulose ester (MCE – pore size 0.8 μm, SKC) filter and imaged (off-line) with phase contrast microscopy (PCM) to measure fiber length distributions. The aerodynamic diameter is also measured by a TSI 3321 Aerosol Particle Sizer (APS) at B. The APS is modified to return the filtered exhaust to a sheath supply within the APS unit while pulling 1.0 lpm from the return. This limits the APS intake to 1.0 lpm with a dilution ratio of 1:1.

Nylon net screens (Millipore Corp., Billerica, MA) with different nominal screen mesh sizes (10, 20, 30, 41, and 60 μm) are loaded in one of the laminar flow chambers indicated at D (Fig. 1) while the other remains empty. The test chambers are conducting tubes and their nominal diameter is 2.5 cm (measured inner diameter 2.2 cm) and total length is 23 cm. Physical properties for nylon net screens used in the study are summarized in Table 1. Screen collection efficiency, η, was obtained from

$$\eta = 1 - \frac{C_{down}}{C_{up}} \tag{1}$$

where C_{up} and C_{down} are the fiber number concentrations of the chamber without and with a screen, respectively. The mean collection efficiency for each fiber length was calculated based on three replicate concentration measurements. Measurement uncertainties are quoted as one standard deviation. Two identical tube chambers (one chamber with a screen and the other without a screen) were used to measure screen collection efficiency. Because identical aerosol paths through the chambers are employed, this approach avoids systematic errors due to particle losses that occur in the chambers to measure particle concentrations with/without a

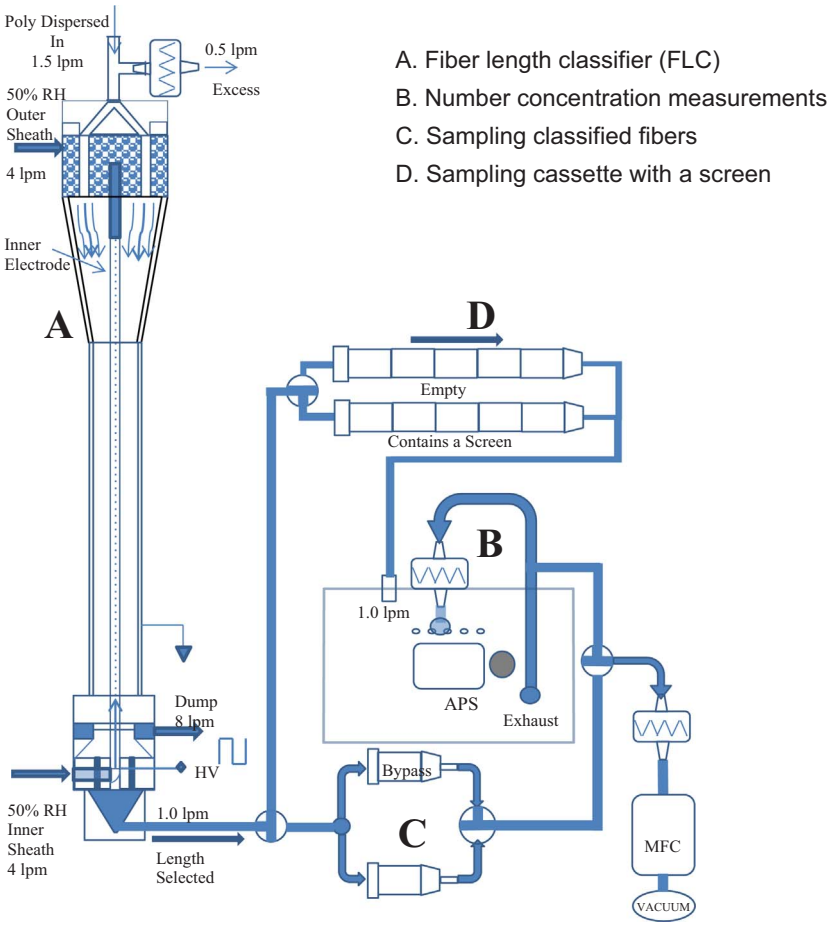

Fig. 1. Experimental setup for monodisperse-length fiber aerosol generation and measurement of screen collection efficiency.

Table 1
Physical properties of nylon net screens used in this study.

Screen pore size (μm)	[a]Fraction of mesh opening area (%)	[b]Thickness (μm)	[c]Solid volume fraction	[d]Screen fiber diameter (μm)
10	4	45	0.778	40
20	14	55	0.536	33
30	17	65	0.499	43
41	31	50	0.426	32
60	41	50	0.318	34

[a] From the manufacturer.
[b] From the manufacturer.
[c] Calculated from measured screen mass and thickness based on Cena, Ku, and Peters (2012).
[d] Calculated from screen pore size and fraction of mesh opening area based on Yamamoto et al. (2005).

screen.

For comparison with the collection efficiency of spherical particles, suspensions of polystyrene latex particles (PSL) (nominal sizes: 1, 2, 3, 5 and 6 μm, Thermo Scientific, Fremont, CA) were electrosprayed using modified spray needles (Ku & Kulkarni, 2009). Comparison of spherical particles with fibers was effected for the 20 μm screen.

3. Results and discussion

3.1. Generation and characterization of monodisperse length aerosol fibers

Fig. 2 shows typical PCM images of glass fibers classified by the dielectrophoresis-based FLC and collected on a MCE filter. Five to ten fields of view along the diameter of the filter were imaged, and lengths of the fibers in all fields were measured using Motic Images Plus 2.0 ML (Motic Instruments, Inc., British Columbia, Canada) (Ku et al., 2014). Typically, the lengths of 100–200 fibers are

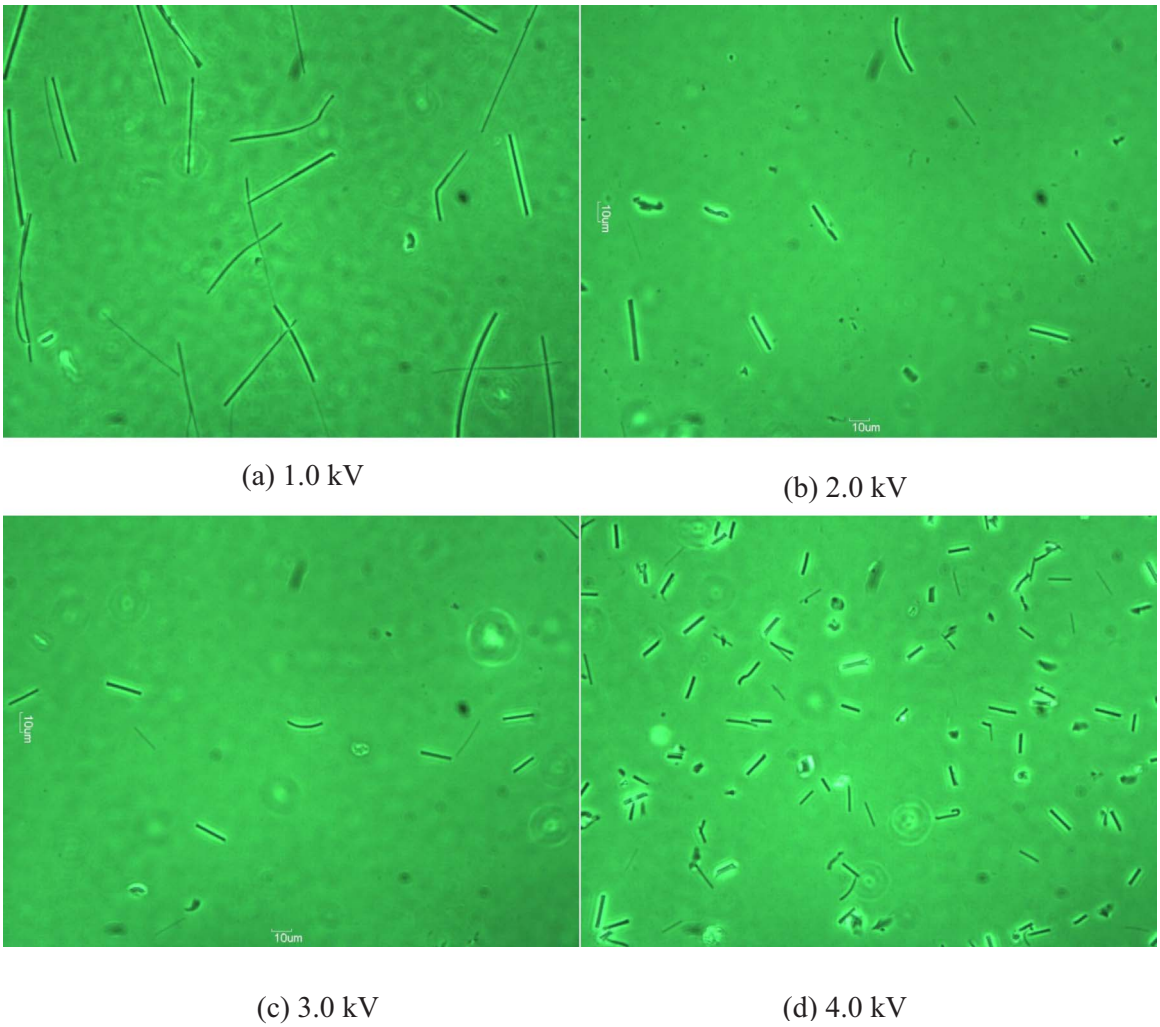

Fig. 2. PCM images of glass fibers classified by the dielectrophoresis-based fiber length classifier for four FLC voltages.

measured. Most of the fibers seem to be straight and well-separated.

As the voltage applied to the FLC is increased, smaller fibers are selected, as shown in Fig. 2. At each applied voltage, fiber lengths were fit to a log-normal length distribution (Fig. 3). Fig. 3a shows a Gauss fit (log-normal fit) of length distributions measured by the PCM at 2 kV; Fig. 3b shows peak-normalized length concentrations for four FLC voltages. The relation of selected fiber length to FLC voltage is tabulated in Table 2, e.g. $V_{FLC} \sim 1$ kV yields fibers of $L \sim 53$ μm; $V_{FLC} \sim 4$ kV yields fibers of $L \sim 11$ μm. The geometric standard deviations are in the range $1.14 < GSD < 1.35$., indicating that the fiber length, as classified by the FLC, is reasonably monodisperse, as shown in previous studies (Baron et al., 1994; Deye et al., 1999). Because these length-classified distributions are relatively narrow, normal and log-normal distributions provide comparable quality fits (in contrast the broad parent aerosol).

Fig. 4 shows the normalized number concentrations of glass fibers, as a function of APS aerodynamic diameter, for each of the four length-classified samples. The statistics of these aerodynamic diameter distributions is given in Table 3. For $V_{FLC} \sim 1$ kV, the mean physical length of the fibers is $L \sim 53$ μm, but the aerodynamic diameter $d_{aero} \sim 2.51$ μm, with $GSD = 1.56$; for $V_{FLC} \sim 4$ kV, the mean physical length if the fibers is $L \sim 11$ μm, but the aerodynamic diameter $d_{aero} \sim 1.08$ μm, with $GSD = 1.72$.

The fiber aerodynamic diameter depends on the fiber physical dimensions (diameter and length) and on the orientation of the fiber in the measuring flow field (Cox, 1970; Hinds, 1999). The physical fiber diameter, d_f, may be calculated by inverting the Cox formulas (Cox, 1970) for aerodynamic diameter

$$d_{\parallel} = d_f \left\{ \frac{9\rho_f}{4\rho_0} [\ln(2\beta) - 0.807] \right\}^{1/2} \tag{2}$$

$$d_{\perp} = d_f \left\{ \frac{9\rho_f}{8\rho_0} [\ln(2\beta) + 0.193] \right\}^{1/2} \tag{3}$$

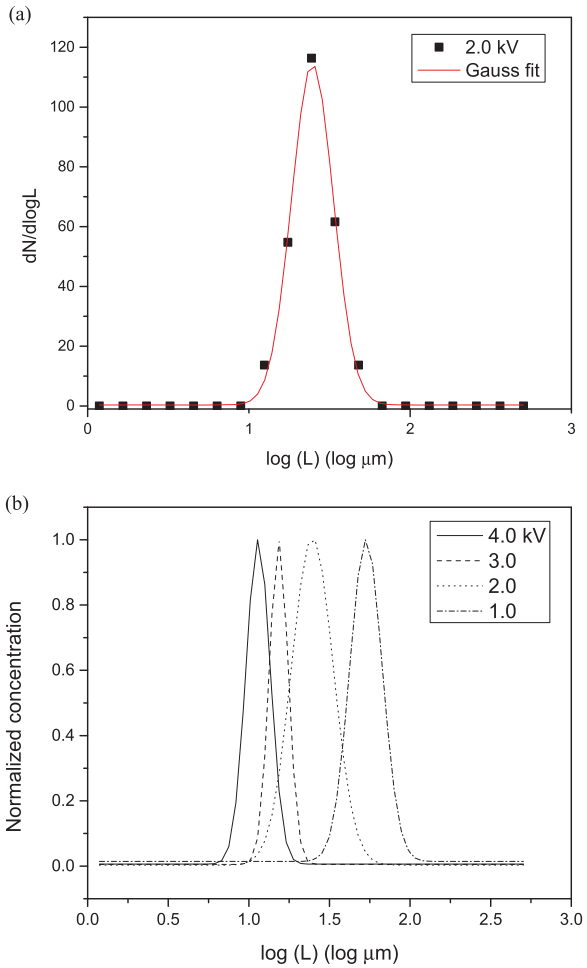

Fig. 3. (a) Typical log-normal length distribution of the glass fibers classified by the FLC, collected on MCE filter. (b) Log-normal length distributions of the classified fibers with four different lengths. The lengths of the fibers were measured using a phase contrast microscope.

Table 2
Geometric mean length, geometric standard deviation and coefficient of variance for fibers classified by the fiber length classifier (FLC).

Voltage applied to FLC (kV)	Geometric mean length (GML, μm)	Geometric standard deviation (GSD)	Coefficient of variation (%)
1.0	53.3	1.26	16.2
2.0	24.8	1.35	14.2
3.0	15.3	1.14	19.2
4.0	11.4	1.19	17.7

where the aspect ratio $\beta = L/d_f$, and the fiber and unit densities are respectively ρ_f and ρ_0. For a random orientation, the aerodynamic diameter is given by:

$$d_{aero} = \frac{(d_{||} + 2d_{\perp})}{3} \tag{4}$$

3.2. Effect of screen mesh size on collection efficiency of fibers

Fig. 5 shows the collection efficiency of screens with different mesh sizes (10, 20, 30, 41, and 60 μm) as a function of aerodynamic diameter for the four different fiber lengths (53, 25, 15, and 11 μm). The indicated error bars represent one standard deviation of three independent measurements.

For the longest fibers (L ~ 53 μm), the coarse screen (mesh size 60 μm) does not efficiently collect fibers (collection efficiency ~ 0.3), but the fine screen (mesh size 10 μm) is quite efficient at collecting fibers (collection efficiency ~ 0.9). For the shortest fibers (L

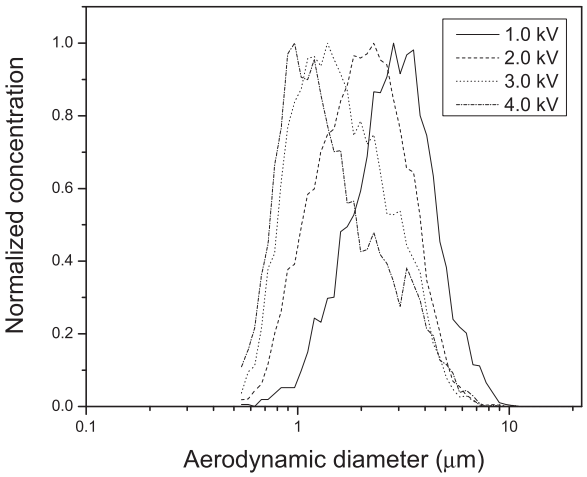

Fig. 4. Normalized number concentration of glass fibers classified by the dielectrophoresis-based fiber length classifier as a function of aerodynamic diameter.

Table 3
Geometric mean diameter, geometric standard deviation and count median diameter for aerodynamic size distributions of the fibers classified by the fiber length classifier.

Voltage applied to FLC (kV)	Geometric mean diameter (GMD, μm)	Geometric standard deviation (GSD)	Count median diameter (CMD, μm)
1.0	2.51	1.56	2.58
2.0	2.21	1.60	2.01
3.0	1.30	1.65	1.53
4.0	1.08	1.72	1.32

~ 11 μm), none of the screens is effective in collecting fibers (collection efficiency ~ 0.1 – 0.3 for 1 μm < d_{aero} < 4 μm).

For the intermediate screens, the collection efficiency profiles are more complicated. For each fiber length, for a given screen, there is a general trend of an increase in collection efficiency with aerodynamic diameter. In the region 1 μm < d_{aero} < 4 μm, all fibers evince a quasi plateau. As a specific example, consider the longest fibers (L ~ 53 μm) and 20 μm screen (Fig. 5b). The collection efficiency rapidly increases for d_{aero} < 1 μm, is nearly constant in the region 1 μm < d_{aero} < 4 μm, and then increases again for d_{aero} > 4 μm. This behavior is observed for these long fibers for screens 30 μm (Fig. 5c), 41 μm (Fig. 5d) and 60 μm (Fig. 5e), with an increase in the upper limit of the plateau with a decrease in screen mesh size.

For fibers with a given length, the aerodynamic diameter depends mostly on fiber diameter. The fact that the collection efficiency is relatively constant in the aerodynamic size range 1–4 μm, for screen 20 and 30, suggests that the fiber collection in this regime mostly depends on the interception of fibers, not on their impaction. If the impaction mechanism were significant, the collection efficiency would increase with increasing aerodynamic diameter (i.e. with fiber diameter). The inertia effect of the fibers seems to start at d_{aero} ~ 4 μm: for d_{aero} > 4–5 μm, the impaction of fibers on the screen seems to be important (Fig. 5b-c) because the collection efficiency starts to increase with increasing aerodynamic diameter (i.e. with increasing fiber diameter). On the other hand, this increase in the collection efficiency is not observed for screen 41 and 60 μm, probably because the mesh size of these screens is not small enough to efficiently collect L ~ 53 μm fibers.

We investigated the length dependence of the screen collection efficiency. Fig. 5a shows the collection efficiency of screen 10 μm for different fiber lengths. As fiber length increases from 11 to 53 μm, the collection efficiency increases. For fibers (53 and 25 μm) larger than the screen mesh size, the collection efficiency is larger than that for fibers (15 and 11 μm) with sizes comparable to the screen size; the collection efficiency is in the range 0.7–1.0, 0.35–0.8, 0.2–0.8 and 0.1–0.8 for each length, respectively as the aerodynamic diameter increases from 0.7 μm to 7–8 μm. For aerodynamic diameters larger than 7–8 μm, the error bar of the collection efficiency becomes large due to the low concentration of the fibers. Nevertheless, the collection efficiency clearly approaches its maximum value (1.0) with increasing aerodynamic diameter. Fig. 5b-e show the collection efficiency of screens 20, 30, 41 and 60 μm for different fiber lengths, respectively. For a given screen mesh size, the collection efficiency generally increases with increasing fiber length. Table 4 summarizes the collection efficiency of each screen for the different fiber lengths.

Fig. 6 shows collection efficiency of long and short fibers as a function of aerodynamic diameter for different screen mesh sizes. For L ~ 53 μm fibers, which are larger than the screen mesh size for all but the 60 μm screen (Fig. 6a), the collection efficiencies increase with increasing aerodynamic diameter, although the pattern of the collection efficiency depends on screen mesh size. On the other hand, for L ~ 11 μm fibers, the collection efficiency is the same for all screen mesh sizes; it is slowly varying for d_{aero} < 2 μm and increases steeply for d_{aero} > 2 μm.

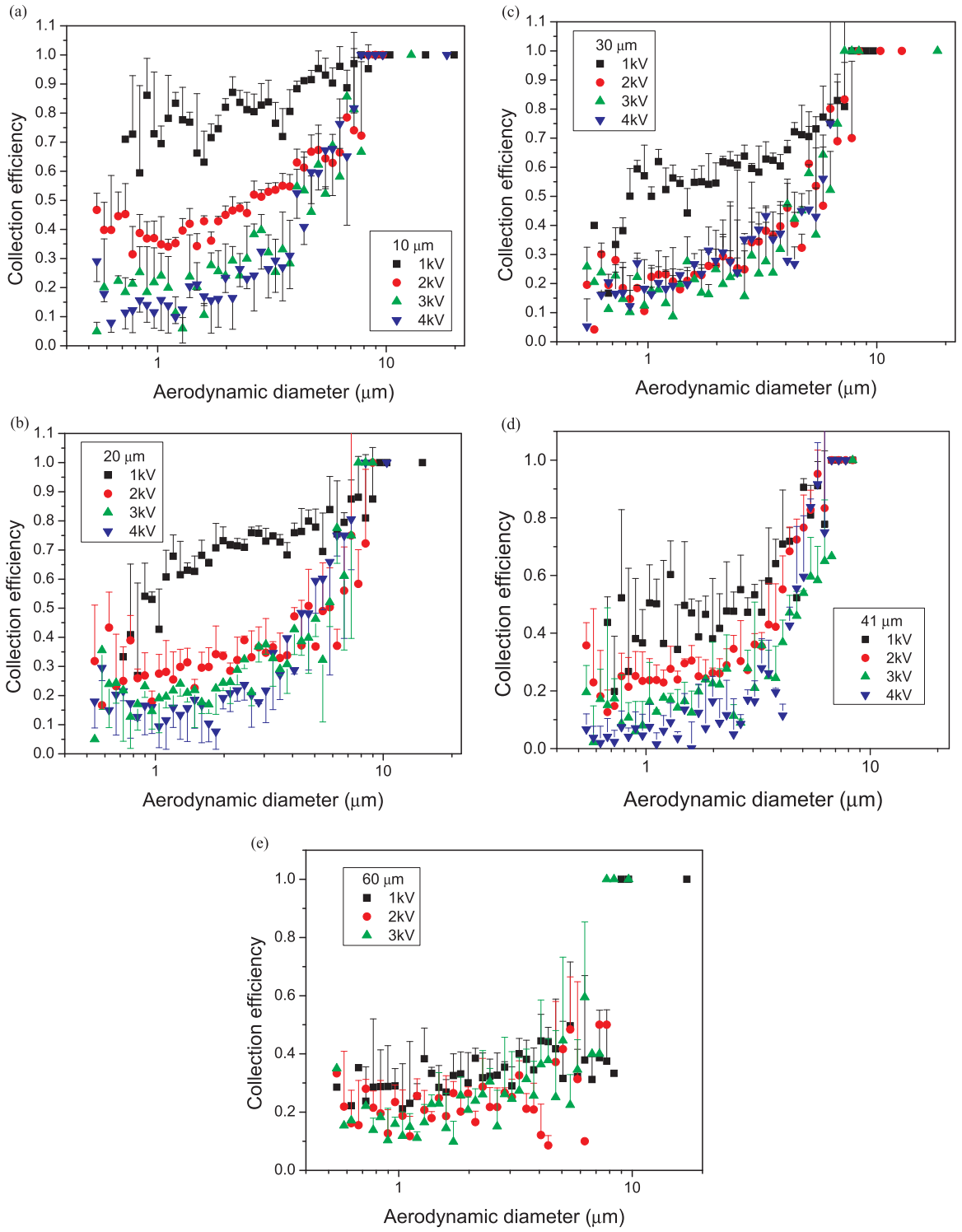

Fig. 5. Collection efficiency of screens [(a) 10, (b) 20, (c) 30, (d) 41 and (e) 60 μm pore sizes] for glass fibers classified by the dielectrophoresis-based fiber length classifier as a function of aerodynamic diameter.

3.3. Effect of fiber diameter on collection efficiency

Fig. 7 shows the collection efficiency of screen 20 μm for classified glass fibers as a function of physical fiber diameter, d_f, for two fiber lengths, 15 μm and 53 μm. The fiber diameter was calculated using (2)–(4) from the measured length and aerodynamic diameter

Table 4
Collection efficiency of each screen for four different fiber lengths in the range from 1.0 to 4.0 μm of aerodynamic diameter.

	Screen mesh size (μm)									
Fiber length (μm)	Ratio of length to mesh size	10	Ratio of length to mesh size	20	Ratio of length to mesh size	30	Ratio of length to mesh size	41	Ratio of length to mesh size	60
53	5.3	0.8–0.9	2.65	0.6–0.7	1.77	0.5–0.6	1.29	0.4–0.5	0.88	0.2–0.4
25	2.5	0.35–0.55	1.25	0.3–0.35	0.83	0.2–0.4	0.61	0.2–0.5	0.42	0.2–0.3
15	1.5	0.2–0.3	0.75	0.2–0.35	0.50	0.2–0.35	0.37	0.2–0.5	0.25	0.15–0.3
11	1.1	0.1–0.3	0.55	0.15–0.25	0.37	0.2–0.35	0.27	0.2–0.5	–	–

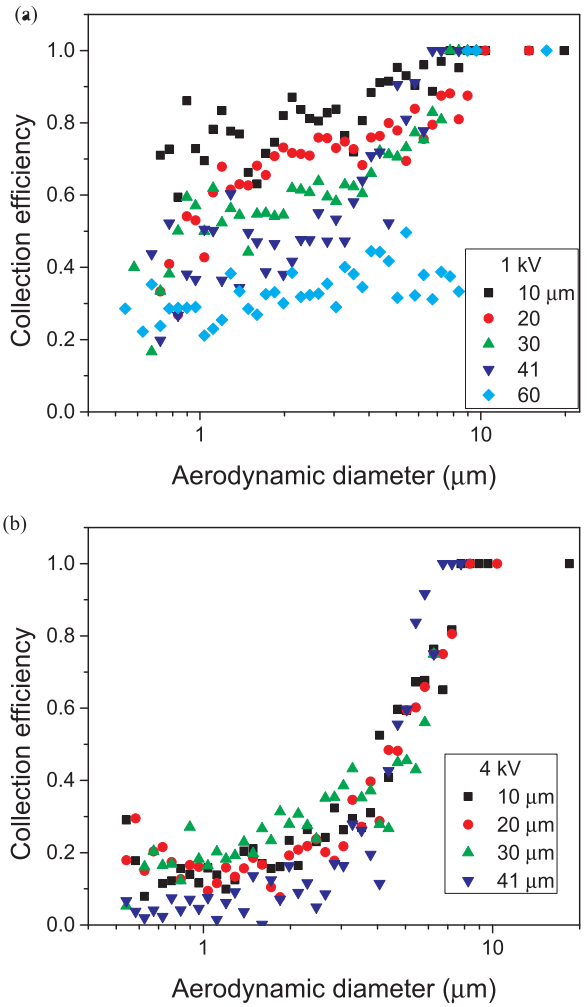

Fig. 6. Collection efficiency of different screens for (a) long (53 μm) and (b) short (11 μm) glass fibers as a function of aerodynamic diameter.

(Cox, 1970). For the longest fibers (L ~ 53 μm), the screen collection efficiency rapidly increases from 0.3 to 0.7, as fiber diameter increases from 0.25μm to 0.5 μm; it then increases moderately from 0.7 to 0.85, as fiber diameter increases from 0.5 to 2.2 μm; for $d_f > 2.2$ μm, the collection efficiency is quite constant. For the shorter fibers (L ~ 15 μm), the collection efficiency varies in a different way: the collection efficiency increases with increasing fiber diameter up to 1.0 μm; it does not change significantly in the fiber diameter range of 1.0–2.0 μm; for $d_f > 2.0$ μm, it increases again with increasing fiber diameter. Compared to the shorter fibers, the longer fibers have a wider range of fiber diameter over which the collection efficiency is constant. The longer fibers are more efficiently collected than the shorter fibers: for 0.5 μm < d_f < 2.5 μm, $\eta_{long} \sim 2\,\eta_{short}$.

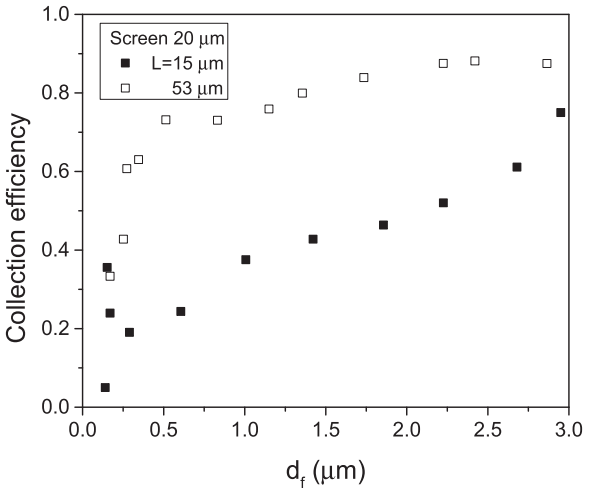

Fig. 7. Collection efficiency of screen 20 μm for length-classified glass fibers as a function of physical fiber diameter (d_f) for long (53 μm) and short (15 μm) fiber lengths. The fiber diameter was calculated from Cox' expression (Cox, 1970) using the measured fiber length and aerodynamic diameter.

3.4. Onset of impaction

Fig. 8 shows collection efficiency of 20 μm screen as a function of Stokes number (Stk). Assuming a negligible slip correction for micron-sized fibers (Hinds, 1999),

$$Stk = \frac{\rho_p d_{aero}^2 U}{18\mu D} \tag{5}$$

where ρ_p is the glass fiber density (2.2 g cm^{-3}), d_{aero} the fiber aerodynamic diameter, D the screen wire diameter (~ 30 μm; Ku et al., 2014), μ the air dynamic viscosity and U the velocity near the screen (~ 7 cm s^{-1}). For the longest fibers, for 0.01 < Stk < 0.1, the collection efficiency increases with Stokes number; for 0.1 < Stk < 0.3, there is a plateau in the collection efficiency; for Stk > 0.4, the collection efficiency increases again. At larger Stk, inertial deposition becomes important. Theoretically, for inviscid (potential) flow around cylinders (Friedlander, 2000), for Stk < 1/8, impaction is negligible. Fig. 8 clearly shows the onset of impaction at Stk ~ 0.2–0.3 (where the collection efficiency starts to increase significantly), in reasonable agreement with the theoretical value of Stk ~ 1/8.

The longest fibers show a different trend of collection efficiency with Stk number compared to the other shorter fibers, as shown in Fig. 8. This result could be explained as follows: In the region 0.01 < Stk < 0.1 in Fig. 8, the longest fibers are supposed to follow flow streamlines with alignment parallel to the flow due to small inertia of the fibers when they penetrate the screen aperture, which makes the collection efficiency small. As Stk number increases in the range of 0.01–0.1, the chance for deviation of the fibers from the air flow streamlines would increase, which makes the collection efficiency increase. In the quasi-plateau region (i.e., 0.1 < Stk <

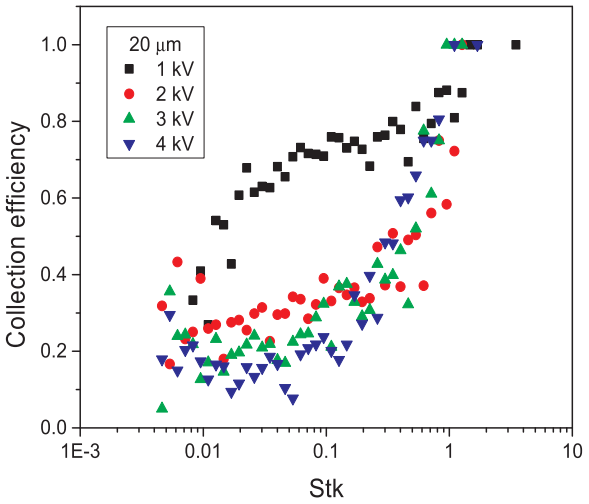

Fig. 8. Collection efficiency of screen 20 μm for length-classified glass fibers as a function of Stokes number based on fiber aerodynamic diameter.

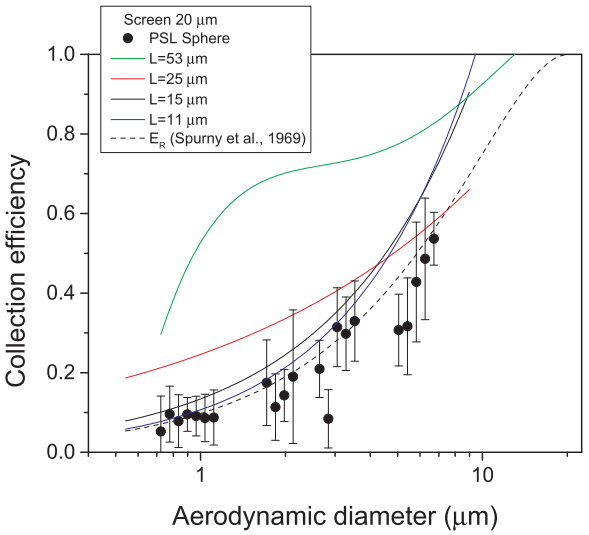

Fig. 9. Comparison of 20 μm screen collection efficiency of length-classified glass fibers to that of spherical particles (polystyrene latex [PSL]) as a function of aerodynamic diameter. The solid lines correspond to curves fitted with experimentally measured collection efficiencies for different fiber lengths. The expression for collection efficiency of interception obtained by Spurny, Lodge, Frank, and Sheesley (1969) is included for comparison.

0.3), the dominant collection mechanism seems to be interception and the collection by interception may occur by frequent flipping of fibers. In the range of Stk > 0.3, it seems that the inertial collection becomes dominant, which is strongly dependent on Stk number.

3.5. Comparison of screen collection efficiency for fibers and spherical particles

Fig. 9 shows 20 μm screen collection efficiency of glass fibers compared to that of size standard spherical particles as a function of aerodynamic diameter. Solid lines in the figure correspond to curves fitted with experimentally measured collection efficiencies for different fiber lengths. The uncertainty of collection efficiency for the size standard PSL spherical particles in Fig. 9 seems to be higher than expected, especially for larger particles (i.e., 6 μm), which is due to the low concentration of airborne PSL particles, even though the data are reproducible. Short fibers, such as 11 and 15 μm, have a collection efficiency comparable to that of spherical particles in the range of 0.7 μm < d_{aero} < 3.0 μm; for d_{aero} > 3.0 μm, they have slightly higher collection efficiency than those of the spherical particles, indicating that short fibers do not contribute to particle collection by interception. However, long fibers, such as 25 and 53 μm show a significantly higher collection efficiency than that of spherical particles for the entire range of aerodynamic diameter; the collection efficiency of the 53 μm fibers is higher than that of the spherical particles by a factor of 2–5. This increase in the collection efficiency is due to enhanced fiber interception by the screen mesh (Spurny, 1986).

Also shown in Fig. 9 is the interception collection efficiency, calculated by the Spurny filtration model (Spurny et al., 1969). This model describes the collection efficiency of the PSL spheres as well as that of the short fibers. This corroborates our conclusion that interception is responsible for the screen collection efficiency of the short fibers (11 μm and 15 μm) over the entire aerodynamic diameter range. As the screen collection efficiency of the long fibers (25 μm and 53 μm) is significantly higher than that predicted by the Spurny model, we conclude that an additional mechanism (e.g. impaction) contributes to their collection by the screen.

3.6. High penetration of long fibers

The low collection efficiency of the screens (i.e., 20 μm and 30 μm) for d_{aero} < 0.8 μm is surprising for the longest fiber (53 μm). With the exception of the 10 μm screen, the collection efficiency of the long fibers is small (~ 0.3) in this aerodynamic range. This may be due to the ease of alignment of the fibers in the air flow when they penetrate the screen apertures; for small aerodynamic diameters, the Stokes number is low (e.g. for d_{aero} ~ 1 μm, Stk ~ 0.02), and the fibers easily follow the air flow streamlines. Chen et al. (2014) reported alignment effect of CNT particles with 30–50 nm in mobility diameter when penetrating through fibrous and electret filter media at a face velocity higher than 10 cm s^{-1}. For 20 μm screen in our study, the superficial velocity that goes through the screen is about 31 cm s^{-1} for aerosol flow rate (1 lpm) and screen opening area fraction (0.14). This may increase penetration of long fibers through the screen in the aerodynamic diameter below 1.0 μm, as shown in Fig. 5b and Fig. 8. However, it should be noted that the CNTs in Chen et al. study are nano-sized, which are much smaller than the glass fibers presently studied and thus, the deposition mechanisms of these two different particles penetrating the screen or filter may be different.

Another factor that may affect the measured collection efficiency is potential fiber flexibility. According to the PCM image analysis, most glass fibers used in this study are rigid and straight (such as those shown in Fig. 2); only a small fraction of the fibers (~ 5–10%), especially the longest fibers, were observed to be very thin and curved. If the longest fibers are bent, due to the high

aerodynamic shear force through the aperture, there may be enhanced penetration through the screen.

3.7. Evaluation of average fiber length collected on the screen

In this section, we attempt to estimate the average fiber length collected on the screens.

The population of fibers in the aerosol is characterized by a joint probability distribution in fiber length, L, and fiber diameter, d_f, or, equivalently, a joint probability distribution, f, in fiber length, L, and aerodynamic diameter, d_{aero}. If these variables were independent, then

$$f(L, d_{aero}) = w(L)g(d_{aero}). \tag{6}$$

i.e. the distribution in aerodynamic diameter would be the same for all classified fiber lengths.

From Fig. 4, it is apparent that, as the fiber length is varied, the distribution in aerodynamic diameter does shift, but only slightly. This motivates approximating the joint probability distribution as

$$f(L, d_{aero}) = \sum_n w_n g_n(d_{aero})\Theta(L_n^- < L < L_n^+) \tag{7}$$

where the 'top-hat' filter function, $\Theta(L^- < L < L^+)$, is unity within, and vanishes outside, the interval $L^- < L < L^+$. We choose to work with normalized distributions $g_n(d_{aero})$. The weights, w_n, are then determined by the experimental cumulants, c_n in the length distribution.

For the 10, 20, 30, 41 μm screens, we have measured collection efficiencies for four classified lengths (11, 15, 25, 53 μm), while for the 60 μm screen, we have only measured collection efficiencies for three classified lengths (15, 25, 53 μm). This necessitates a trivial modification for this last screen. For the four length approximation, we take

$$L_1^- = 0, L_1^+ = \frac{L_1 + L_2}{2} = L_2^-, L_2^+ = \frac{L_2 + L_3}{2} = L_3^-, L_3^+ = \frac{L_3 + L_4}{2} = L_4^-, L_4^+ = L_{max}, \tag{8a}$$

where we have introduced an upper cut-off length, L_{max}. Similar formulas obtain for the three length approximation

$$L_1^- = 0, L_1^+ = \frac{L_1 + L_2}{2} = L_2^-, L_2^+ = \frac{L_2 + L_3}{2} = L_3^-, L_3^+ = L_{max}, \tag{8b}$$

The weights, w_n, are determined from the length cumulants, c_n, of the distribution

$$\begin{aligned} w_1 \frac{L_1 + L_2}{2} &= c_1 \\ w_2 \frac{L_3 - L_1}{2} &= c_2 \\ w_4 \frac{L_4 - L_2}{2} &= c_3 \\ w_4 \frac{(2L_{max} - L_3 - L_4)}{2} &= c_4 \end{aligned} \tag{9a}$$

Similar formulas obtain for the three length approximation

$$\begin{aligned} w_1 \frac{L_1 + L_2}{2} &= c_1 \\ w_2 \frac{L_3 - L_1}{2} &= c_2 \\ w_3 \frac{(2L_{max} - L_2 - L_3)}{2} &= c_3 \end{aligned} \tag{9b}$$

The average length in the aerosol, $< L >$, is given by

$$4<L> = (c_1 + c_2)L_1 + (c_1+2c_2 + c_3)L_2 + (c_2+2c_3 + c_4)L_3 + (c_3 + c_4)L_4+2c_4L_{max}. \tag{10a}$$

The measured average length in the aerosol, $< L > = 30.1$ μm, determines the upper cut-off to be $L_{max} = 108.7$ μm. Similarly, for the three length approximation,

$$4<L> = (c_1 + c_2)L_1 + (c_1+2c_2 + c_3)L_2 + (c_2 + c_3)L_3 + (c_3 + c_4)L_4+2c_3L_{max}. \tag{10b}$$

determines a similar upper cut-off length $L_{max} = 109.2$ μm.

The average length of the fibers collected on the screens is given by

$$4<L>_{screen} = \frac{[(b_1 + b_2)L_1 + (b_1+2b_2 + b_3)L_2 + (b_2+2b_3 + b_4)L_3 + (b_3 + b_4)L_4+2b_4L_{max}]}{[b_1 + b_2 + b_3 + b_4]}, \tag{11a}$$

where

$$b_n = c_n \int \eta_n(d_{aero})g_n(d_{aero})dd_{aero} \tag{12}$$

and where $\eta_n(d_{aero})$ is the efficiency function for fibers of length L_n. A similar formula obtains for the three length approximation

$$4<L>_{screen} = \frac{[(b_1 + b_2)L_1 + (b_1+2b_2 + b_3)L_2 + (b_2 + b_3)L_3+2b_3L_{max}]}{[b_1 + b_2 + b_3]} \quad (11b)$$

Within this model, we obtain the average lengths collected on each screen

$$\begin{aligned} <L>_{10\mu m} &= 37.6\mu m \\ <L>_{20\mu m} &= 43.1\mu m \\ <L>_{30\mu m} &= 40.4\mu m \\ <L>_{41\mu m} &= 43.2\mu m \\ <L>_{60\mu m} &= 35.6\mu m \end{aligned} \quad (13)$$

This is to be compared with $< L > = 30.1$ μm for the parent aerosol stream, i.e. the average length on the screens is 20–45% higher. Thus the screens have the effect of preferentially capturing the longer fibers, although our measurements have not determined any systematic variation with screen mesh size.

As a final remark, the method presented in the study to estimate average fiber length based on the screen collection efficiency shows the potential that the measured collection efficiencies can be used to estimate the mean length. However, the accuracy for this approach needs to be further investigated for the future to determine whether the approach would be reliable for different fiber materials by directly measuring the lengths of fibers collected on the screen.

4. Conclusion

We investigated screen collection efficiency of airborne fibers with monodisperse length. This is the first study to quantitatively determine the efficacy of screens to capture fibers from an airstream, as a function of fiber length. As such, it represents a fundamental advance in the understanding of the interaction of screens with a fibrous aerosol.

Monodisperse length fibers were prepared by a dielectrophoresis-based fiber length classifier. The collection efficiency of screens with different mesh sizes was obtained by measuring the fiber concentrations upstream and downstream of the screens. The collection efficiency for the fibers was compared to that of spherical particles. We conclude the following based on this study.

1. As the screen mesh size decreases from 60 μm to 10 μm, the screen collection efficiency increases from 0.3 to 0.9 for the longest fibers (~ 53 μm) in the range of 1–4 μm in aerodynamic diameter.
2. The collection efficiency for fibers with a given physical length is nearly constant in the range of aerodynamic diameters 1 μm < d_{aero} < 4 μm for screen 20 and 30 μm, but it rises significantly at aerodynamic diameters larger than 4 μm.
3. The collection efficiency is due to fiber interception in the plateau regime (1 μm < d_{aero} < 4 μm) and fiber impaction for d_{aero} > 4 μm.
4. The collection efficiency of screen 20 μm for fibers with lengths > 20 μm is a factor of two to five larger than that for spherical particles with the same aerodynamic diameter.
5. The average fiber length collected on the screens is 20–45% longer than the average fiber length in the parent aerosol.

Disclaimer

Mention of a company name or product does not constitute endorsement by the Centers for Disease Control and Prevention. The findings and conclusions in this paper are those of the authors and do not necessarily represent the views of the National Institute for Occupational Safety and Health.

Acknowledgments

The authors would like to thank Emanuele Cauda and Yung-Sung Cheng for their helpful comments on this work, and thank Mariko Ono-Ogasawara (Japan NIOSH) for the samples of the glass fibers. This work was funded by the US National Institute for Occupational Safety and Health under the NORA project (CAN 7939ZXEM).

References

Bahk, Y. K., Buha, J., & Wang, J. (2013). Determination of geometrical length of airborne carbon nanotubes by electron microscopy, model calculation and filtration method. *Aerosol Science and Technology, 47*, 776–784.
Baron, P. A. (2001). Measurement of airborne fibers: A review. *Industrial Health, 39*, 39–50.
Baron, P. A., Deye, G. J., & Fernback, J. (1994). Length separation of fibers. *Aerosol Science and Technology, 21*(2), 179–192.
Cena, L. G., Ku, B. K., & Peters, T. M. (2012). Particle collection efficiency for nylon mesh screens. *Aerosol Science and Technology, 46*(2), 214–221.
Chen, S.-C., Wang, J., Bahk, Y. K., Fissan, H., & Pui, D. Y. H. (2014). Carbon nanotube penetration through fiberglass and electret respirator filter and nuclepore filter media: Experiments and models. *Aerosol Science and Technology, 48*(10), 997–1008.
Cox, R. G. (1970). The motion of long slender bodies in a viscous fluid I: General theory. *Journal of Fluid Mechanics, 44*, 791–810.
Deye, G. J., Gao, P., Baron, P. A., & Fernback, J. (1999). Performance evaluation of a fiber length classifier. *Aerosol Science and Technology, 30*, 420–437.
Friedlander, S. K. (2000). *Smoke, dust, and haze.* New York, NY: Oxford University Press.

Gentry, J. W., & Spurny, K. R. (1978). Measurements of collection efficiency of nuclepore filters for asbestos fibers. *The Journal of Colloid and Interface Science, 65*, 174.
Gentry, J. W., Spurny, K. R., Opiela, H., & Weiss, G. (1980). Measurement of collection efficiency of amosite fibers. *Industrial & Engineering Chemistry Product Research and Development, 19*(1), 47–52.
Gentry, J. W., Spurny, K. R., & Schoermann, J. (1989). Collection efficiency of ultrafine asbestos fibers. Experiment and theory. *Aerosol Science and Technology, 8*, 184–195.
Hesterberg, T. W., & Hart, G. A. (2001). Synthetic vitreous fibers: A review of toxicology research and its impact on hazard classification. *Critical Reviews in Toxicology, 31*(1), 1–53.
Hinds, W. C. (1999). *Aerosol technology: Properties, behavior, and measurement of airborne particles.* New York, USA: John Wiley & Sons.
Kohyama, N., Tanaka, I., Tomita, M., Kudo, M., & Shinohara, Y. (1997). Preparation and characteristics of standard reference samples of fibrous minerals for biological experiments. *Industrial Health, 35*, 415–432.
Ku, B. K., Deye, G., & Turkevich, L. A. (2013). Characterization of a vortex shaking method for aerosolizing fibers. *Aerosol Science and Technology, 47*(12), 1293–1301.
Ku, B. K., Deye, G. J., & Turkevich, L. A. (2014). Efficacy of screens in removing long fibers from an aerosol stream – Sample preparation technique for toxicology studies. *Inhalation Toxicology, 26*(2), 70–83.
Ku, B. K., & Kulkarni, P. (2009). Morphology of single-wall carbon nanotube aggregates generated by electrospray of aqueous suspensions. *Journal of Nanoparticle Research, 11*, 1393–1403.
Lipowicz, P. J., & Yeh, H. C. (1989). Fiber dielectrophoresis. *Aerosol Science and Technology, 11*(3), 206–212.
Myojo, T. (1999). A simple method to determine the length distribution of fibrous aerosols. *Aerosol Science and Technology, 30*, 30–39.
NIOSH (2011). *Asbestos fibers and other elongate mineral particles: State of the science and roadmap for research* [DHHS (NIOSH) Publication No. 2011-2159]. ⟨http://www.cdc.gov/niosh/docs/2011-159/pdfs/2011-159.pdf⟩.
Spurny, K. R. (1986). On the filtration of fibrous aerosols. *Science of The Total Environment, 52*(3), 189–199.
Spurny, K. R., Lodge, J. P., Jr., Frank, E. R., & Sheesley, D. C. (1969). Aerosol filtration by means of Nuclepore filters: Structural and filtration properties. *Environmental Science & Technology, 3*(5), 453–464.
Spurny, K. R., Stober, W., Opiela, H., & Weiss, G. (1979). Size-selective preparation of inorganic fibers for biological experiments. *American Industrial Hygiene Association Journal, 40*, 20–38.
Stanton, M. F., Layard, M., Tegeris, A., Miller, E., May, M., Morgan, E., & Smith, A. (1981). Relation of particle dimension to carcinogenicity in amphibole asbestoses and other fibrous minerals. *Journal of the National Cancer Institute, 67*, 965–975.
Su, W. C., & Cheng, Y. S. (2005). Deposition of fiber in the human nasal airway. *Aerosol Science and Technology, 39*, 888–901.
Su, W. C., & Cheng, Y. S. (2006). Deposition of fiber in a human airway replica. *Journal of Aerosol Science, 37*(11), 1429–1441.
Su, W. C., & Cheng, Y. S. (2009). Deposition of man-made fibers in human respiratory airway casts. *Journal of Aerosol Science, 40*(3), 270–284.
Su, W. C., Wu, J., & Cheng, Y. S. (2008). Deposition of man-made fiber in a human nasal airway. *Aerosol Science and Technology, 42*(3), 73–181.
Wang, Z., Hopke, P. K., Baron, P. A., Ahmadi, G., Cheng, Y.-S., Deye, G., & Su, W.-C. (2005). Fiber classification and the influence of average air humidity. *Aerosol Science and Technology, 39*(11), 1056–1063.
Yamamoto, N., Kumagai, K., Fujii, M., Shendell, D. G., Endo, O., & Yanagisawa, Y. (2005). Size-dependent collection of micrometer-sized particles using nylon mesh. *Atmospheric Environment, 39*, 3675–3685.